AGU PUBLICATIONS

JGR

Journal of Geophysical Research: Atmospheres

RESEARCH ARTICLE
10.1002/2015JD024700

Changes in precipitating snow chemistry with location and elevation in the California Sierra Nevada

Jessie M. Creamean[1,2], Jessica L. Axson[3], Amy L. Bondy[4], Rebecca L. Craig[4], Nathaniel W. May[4], Hongru Shen[3], Michael H. Weber[4], Kerri A. Pratt[4,5], and Andrew P. Ault[3,4]

[1]Cooperative Institute for Research in Environmental Sciences, University of Colorado Boulder, Boulder, Colorado, USA, [2]Physical Sciences Division, NOAA Earth System Research Laboratory, Boulder, Colorado, USA, [3]Department of Environmental Health Sciences, University of Michigan, Ann Arbor, Michigan, USA, [4]Department of Chemistry, University of Michigan, Ann Arbor, Michigan, USA, [5]Department of Earth and Environmental Sciences, University of Michigan, Ann Arbor, Michigan, USA

Jessie M. Creamean and Jessica L. Axson contributed equally to this work.

Key Points:
- Physiochemical properties of particles found in precipitation were determined
- Both anthropogenic and natural sources contributed to the snow residue chemistry
- Snow residue sources varied depending on location and elevation

Supporting Information:
- Supporting Information S1

Correspondence to:
J. M. Creamean and A. P. Ault,
jessie.creamean@colorado.edu;
aulta@umich.edu

Citation:
Creamean, J. M., J. L. Axson, A. L. Bondy, R. L. Craig, N. W. May, H. Shen, M. H. Weber, K. A. Pratt, and A. P. Ault (2016), Changes in precipitating snow chemistry with location and elevation in the California Sierra Nevada, *J. Geophys. Res. Atmos.*, *121*, 7296–7309, doi:10.1002/2015JD024700.

Received 8 JAN 2016
Accepted 9 JUN 2016
Accepted article online 13 JUN 2016
Published online 30 JUN 2016

Abstract Orographic snowfall in the Sierra Nevada Mountains is an important source of water for California and can vary significantly on an annual basis. The microphysical properties of orographic clouds and subsequent formation of precipitation are impacted, in part, by aerosols of varying size, number, and chemical composition, which are incorporated into clouds formed along the Sierra barrier. Herein, the physicochemical properties and sources of insoluble residues and soluble ions found in precipitation samples were explored for three sites of variable elevation in the Sierra Nevada during the 2012–2013 winter season. Residues were characterized using a suite of physicochemical techniques to determine the size-resolved number concentrations and associated chemical composition. A transition in the aerosol sources that served as cloud seeds or were scavenged in-cloud and below-cloud was observed as a function of location and elevation. Anthropogenic influence from the Central Valley was dominant at the two lowest elevation sites (1900 and 2200 m above mean sea level (AMSL)), whereas long-range transported mineral dust was a larger contributor at the highest elevation site where cleaner conditions were observed (2600 m AMSL). The residues and soluble ions observed provide insight into how multiple aerosol sources can impact cloud and precipitation formation processes, even over relatively small spatial scales. The transition with increasing elevation to aerosols that serve as ice nucleating particles may impact the properties and extent of snowfall in remote mountain regions where snowpack provides a vital supply of water.

1. Introduction

Orographic snowfall, which increases snowpack, plays a key role in providing water to reservoirs in California and other regions with limited water resources [*Borys et al.*, 2000; *Dettinger et al.*, 2011]. Winter storms, particularly those produced from atmospheric rivers (i.e., narrow, meridional bands of concentrated water vapor from the tropics), can contribute up to 50% of California's annual precipitation and 72% of snow water equivalent in the Sierra Nevada [*Dettinger et al.*, 2011; *Guan et al.*, 2012]. Additionally, these storms are impacted by aerosols originating from both regional and global sources, which modify the amount and location of precipitation [*Ault et al.*, 2011; *Creamean et al.*, 2014a, 2015, 2013; *Fan et al.*, 2014; *Lynn et al.*, 2007; *Rosenfeld et al.*, 2014; *Xiao et al.*, 2014]. In particular, certain aerosol particles can modify ice crystal formation and subsequent intensity, phase, and location of precipitation [*Andreae and Rosenfeld*, 2008, 2004, 2007; *Pruppacher and Klett*, 1978; *Saleeby et al.*, 2009]. Changes in annual precipitation from natural [*Guan et al.*, 2012] or anthropogenic [*Rosenfeld et al.*, 2008] precipitation formation processes in the Sierra Nevada have the potential to impact millions of people. Thus, it is important to understand the sources of aerosols that influence ice and mixed phase cloud formation and subsequent snowfall in the Sierra Nevada.

The chemical and physical properties of aerosols involved in precipitation processes are an important component in understanding aerosol sources and aerosol-cloud-precipitation interactions impacting orographic snowfall. Several studies have utilized bulk soluble components of precipitation to elucidate sources and atmospheric processing of aerosols involved in precipitation [*Henning et al.*, 2003; *Lafreniere and Sinclair*, 2011; *Shrestha et al.*, 1997; *Sorooshian et al.*, 2013; *Xu et al.*, 2014]. However, the primary aerosols that act as ice nucleating particles (INPs)—mineral dust, soot, and primary biological particles—are typically insoluble, irregularly shaped, and relatively large compared to particles that are poor INPs, such as those originating

from pollution (i.e., containing sulfate or nitrate) [*Andreae and Rosenfeld*, 2008; *Christner et al*., 2008; *Creamean et al*., 2013; *Klein et al*., 2010; *Sullivan et al*., 2007, 2010]. These effective INPs contain surface sites that enable ice crystal formation at temperatures higher than homogeneous nucleation (−36 °C) [*Pruppacher and Klett*, 1978; *Vali et al*., 2015]. In mixed-phase clouds, these ice crystals can then rapidly form and successively enhance precipitation through collision and coalescence with supercooled cloud droplets [*Bergeron*, 1935; *Hallett et al*., 1978; *Mossop*, 1970; *Mossop et al*., 1970]. Additionally, the falling precipitation can scavenge below-cloud aerosols, though to a lesser extent than in-cloud scavenging, which further alters the chemical composition of the precipitation [*Croft et al*., 2009, 2010; *Radke et al*., 1980; *Rodhe and Grandell*, 1972; *Schumann et al*., 1988]. *Croft et al*. [2009] determined size dependent below-cloud scavenging coefficients for sea salt, dust, black carbon, particulate organic matter, and sulfate particles, showing that primarily sea salt would be affected by below-cloud scavenging, whereas particulate sulfate and nitrate were observed to be predominantly affected by in-cloud scavenging [*Croft et al*., 2009; *Kasper-Giebl et al*., 1999]. However, globally, only approximately 10–15% of aerosols are scavenged as compared to serving as cloud droplet or ice crystal nuclei. Thus, the physiochemical properties of insoluble residues in precipitation can provide knowledge of the in-cloud INPs and the extent to which these particles potentially impact precipitation formation.

The analysis of single particles enables the identification of individual sources of aerosols that influence cloud and precipitation formation [*Ault et al*., 2011; *Axson et al*., 2016; *Creamean et al*., 2015, 2014b, 2013; *Holecek et al*., 2007; *Ma et al*., 2004; *Matthias-Maser et al*., 2000; *Schutz and Kramer*, 1987; *Zhang et al*., 2013]. Given that INPs are typically insoluble particles, analysis of single particles provides an advantage over bulk solution analysis as it is possible to analyze individual insoluble residues from snowmelt to determine their sources. *Creamean et al*. [2014b] investigated the chemical composition of both soluble ions and insoluble residues from samples collected during three consecutive winter seasons in the California Sierra Nevada using ion chromatography and single-particle mass spectrometry. From that work, detailed residue classification criteria were developed based on field samples and controlled laboratory experiments of known materials, including dust, biomass smoke, leaf litter, and sea salt [*Creamean et al*., 2014b]. In combination with soluble ion chemistry, insoluble residue size and chemical composition can be used to help unravel aerosol-cloud-precipitation interactions. To date, this type of integrated analysis has only been conducted using samples from one location in the northern Sierra Nevada, Sugar Pine Dam (39.13°N, 120.80°W). Thus, the impact of insoluble residues on orographic cloud and precipitation formation processes at additional locations, and at different elevations, along the Sierra remains uncertain.

The current study examined the physicochemical properties and sources of potential INPs that impact the Sierra Nevada at different locations and elevations. Freshly fallen snow samples were collected at three sites in Yosemite National Park, California during the 2012–2013 winter season. Residue chemistry, size, and morphology along with soluble ion chemistry were evaluated for the melted snow samples using a comprehensive suite of analytical instrumentation including both bulk and single-particle methods. Air mass trajectory analysis was utilized to determine the potential source regions of the measured residues. Together, these analyses provided information regarding the origin and atmospheric processing of insoluble residue particles and soluble ions, as well as information regarding potential effects on precipitation at varying elevations in the California Sierra Nevada. Deciphering the sources and properties of precipitation residue particles involved with aerosol-cloud-precipitation interactions in this region is critical to assessing future availability of water resources.

2. Materials and Methods

2.1. Snow Collection

Fresh fallen snow was collected as the snow precipitated (i.e., prior to reaching the ground) during the winter of 2012–2013 at three locations in Yosemite National Park. The preferential capture of larger snow crystals during moderate wind conditions was possible; however, unless there was a strong size dependence for uptake of aerosols with specific size and composition, this is not likely to have a significant effect on the results [*Pomeroy et al*., 1991]. Snow sample collection start and end times are provided in Table S1 of the supporting information. The sites for sample collection are shown in Figure 1 including Crane Flat (CFT; 1900 m above mean sea level (m AMSL); 38.11°N, 119.84°W), Badger Pass (BPS; 2200 m AMSL;

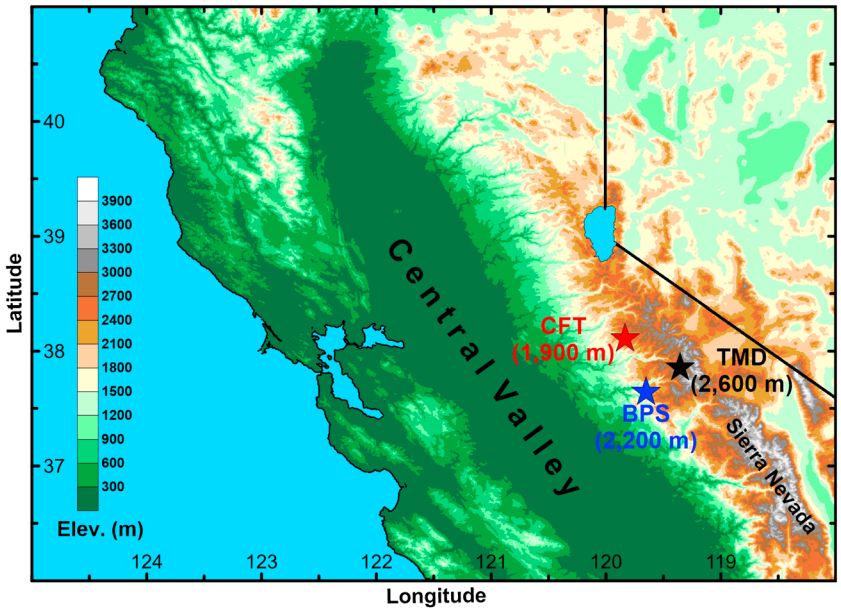

Figure 1. Map of sites in Yosemite National Park, California where snow samples were collected. Sites include Crane Flat (CFT), Badger Pass (BPS), and Tuolumne Meadows (TMD).

37.67°N, 119.65°W), and Tuolumne Meadows (TMD; 2600 m AMSL; 37.87°N, 119.36°W). Due to sample volume limitations, insoluble sizing and chemical analysis was not performed on the December TMD sample, and only results from ion chromatography are discussed. Snow samples were collected in 5 gal polytetrafluoroethylene (PTFE)-lined bags during snowfall and sealed with a polytetrafluoroethylene (PTFE) clip. Samples were then kept frozen in a standard commercial freezer and stored for approximately 14–15 months until analysis. Prior to any analysis, each sample was completely melted and rigorously stirred/agitated in order to redistribute insoluble residues which may have settled during thawing.

2.2. Sizing of Insoluble Residues in Melted Snow

An LM10 (Nanosight™) nanoparticle tracking analysis (NTA) was used to determine the number concentration and size distribution of submicron (0.01–1.0 μm in diameter) insoluble residue particles present in the melted snow samples. The method is described in detail in *Axson et al.* [2014]. Coagulation of particles in solution, is not expected based on control studies of snow sample NTA analysis conducted and discussed by *Axson et al.* [2016]. Prior to the injection of each sample, a 10 s video of the NTA cell containing 18 MΩ MilliQ water was acquired as a blank for cell cleanliness. A 500 μL aliquot of each sample was used, of which 350 μL was loaded into the LM10 cell using a 1 mL syringe and 11 × 30 s videos of the insoluble residues were captured. All samples were run in triplicate. Sample videos were batch processed after each experiment using Nanosight NTA 3.0 (Build 60) software providing the particulate distribution in terms of size versus number concentration (cm^{-3}) for each sample. Raw data for the insoluble residue number concentration and size distributions are provided in 64 bins/decade.

2.3. Raman Microspectroscopy of Dried Residues

A Raman microspectrometer (LabRAM HR Evolution; Horiba Scientific) was used to obtain vibrational spectra and projected area diameter of residues dried on quartz substrates. The Raman microspectrometer was equipped with a confocal optical microscope with a 100X objective, Nd:YAG laser (50 mW, 532 nm), and CCD detector. Prior to use, the Raman was calibrated against pure Si with a Raman signal at 520 cm^{-1}. A 600 g mm^{-1} diffraction grating was used to allow for a spectral resolution of approximately 2.0 cm^{-1}. A 1 μL drop of each of the melted snow samples was placed on separate quartz substrates and allowed to dry overnight in a closed environment at room temperature (22°C). The LabSpec 6 software Particle Finder module (Horiba Scientific) was used to collect several images and spectra of the dried residues. Raman spectra of the residues were collected between 100 and 4000 cm^{-1} with a 100% transmission neutral density filter

Table 1. Descriptions of All the Analytical Methods Used on the Yosemite Samples, Including Nanoparticle Tracking Analysis (NTA), Raman Microspectroscopy, Scanning Electron Microscopy With Energy Dispersive X-Ray Spectrometry (SEM/EDX), and Ion Chromatography (IC)

Method	Purpose	Size Range (μm)	Number of Residues Analyzed
NTA	Insoluble residue size and concentration in solution	0.01–1.0	875 residues/video
Raman[a]	Residue size, morphology, and chemical functional groups	>1	591 residues
SEM/EDX[a]	Residue size, morphology, and elemental composition	0.003–30[b]	119 residues
IC	Bulk soluble ion composition and quantification	–	–

[a]Actual measured size ranges are presented in the supporting information Figures S1 and S2.
[b]Represents theoretical size range of instrument and not actual measured ranged due to instrument configurations for sample.

at 1 s acquisitions for two accumulations. Divisive clustering analysis was then used to classify and identify particles based on distinct features in each spectrum and comparison with prior studies using Raman microspectroscopy [*Ault et al*., 2013a, 2014; *Craig et al*., 2015].

2.4. Scanning Electron Microscopy (SEM) of Dried Residues

Dried residues from melted snow samples were analyzed using scanning electron microscopy (SEM), specifically an FEI Quanta environmental dual FIB/SEM equipped with a tungsten filament operating at 20 kV and a secondary electron detector. The instrument was equipped with an energy dispersive X-ray (EDX) spectrometer (EDAX, Inc.), which allowed for X-ray detection of elements with atomic numbers higher than beryllium. Samples were prepared by depositing a 1 μL drop of each melted snow sample on individual silicon wafers and allowing them to dry overnight in a closed environment at room temperature (22°C). Secondary electron images were captured along with corresponding EDX spectra for individual dried residues from each of the melted snow samples. The images and spectra were then used to identify characteristic dried residue types as described by *Axson et al*. [2016]. An extensive list of aerosol sources and their representative EDX spectra, from which the insoluble types were identified, are given in *Ault et al*. [2012] and *Shen et al*. [2016].

2.5. Ion Chromatography (IC) of Soluble Ions in Melted Snow

Dionex ICS-1100 and ICS-2100 ion chromatographs were used to analyze the soluble ions in the melted snow samples. These ions include ammonium (NH_4^+), calcium (Ca^{2+}), magnesium (Mg^{2+}), potassium (K^+), sodium (Na^+), chloride (Cl^-), nitrate (NO_3^-), and sulfate (SO_4^{2-}). Further details including the limits of detection are provided in the supporting information (Table S2). Methanesulfonic acid (20 mM) was used as eluent for the cation column, and KOH gradient generated by an EGC III KOH system was used as eluent for the anion column. For both the cation and anion analysis, 1 mL aliquots of the samples were used, and all samples were run in triplicate. For the correlation analysis, the total concentration of ions for all of the samples was compared as a whole.

2.6. Definition of Terms: Insoluble Residue, Dried Residue, and Soluble Ions

Details of each method for residue and soluble ion analysis of the melted snow have been compiled in Table 1. Melted snow samples were analyzed for size and chemical composition either in solution or after drying on substrates. It is important to clearly delineate the different terms for the types of particles or particle components analyzed by each method. NTA analyzes insoluble residues (no soluble components), Raman and SEM/EDX analyze dried residues that include both insoluble particles and soluble components, and IC analyzes soluble components only. Other caveats associated with drying of insoluble resides are discussed in detail by *Creamean et al*. [2014b]. When interpreting insoluble residue sources, only insoluble components of the residues (i.e., dust and organic carbon) were used to determine the primary sources of the dried residues, while bulk soluble ion analysis was used to characterize the extent of aged aerosol present.

2.7. Air Mass Back Trajectory Analysis

To examine possible aerosol source regions and transport pathways, air mass back trajectory analysis was conducted using Hybrid Single-Particle Lagrangian Integrated Trajectory (HYSPLIT) 4 [*Draxler and Rolph*, 2011] with archived meteorological field data (1° resolution) from the National Centers for Environmental Prediction Global Data Assimilation System [*Kalnay et al*., 1996]. An ensemble of back trajectories were initiated every 3 h at multiple altitudes above each sample collection site and included 10 day trajectories during snowfall at 0, 50, 100, 500, 1000, 2000, 3000, 4000, 5000, 6000, 7000, and

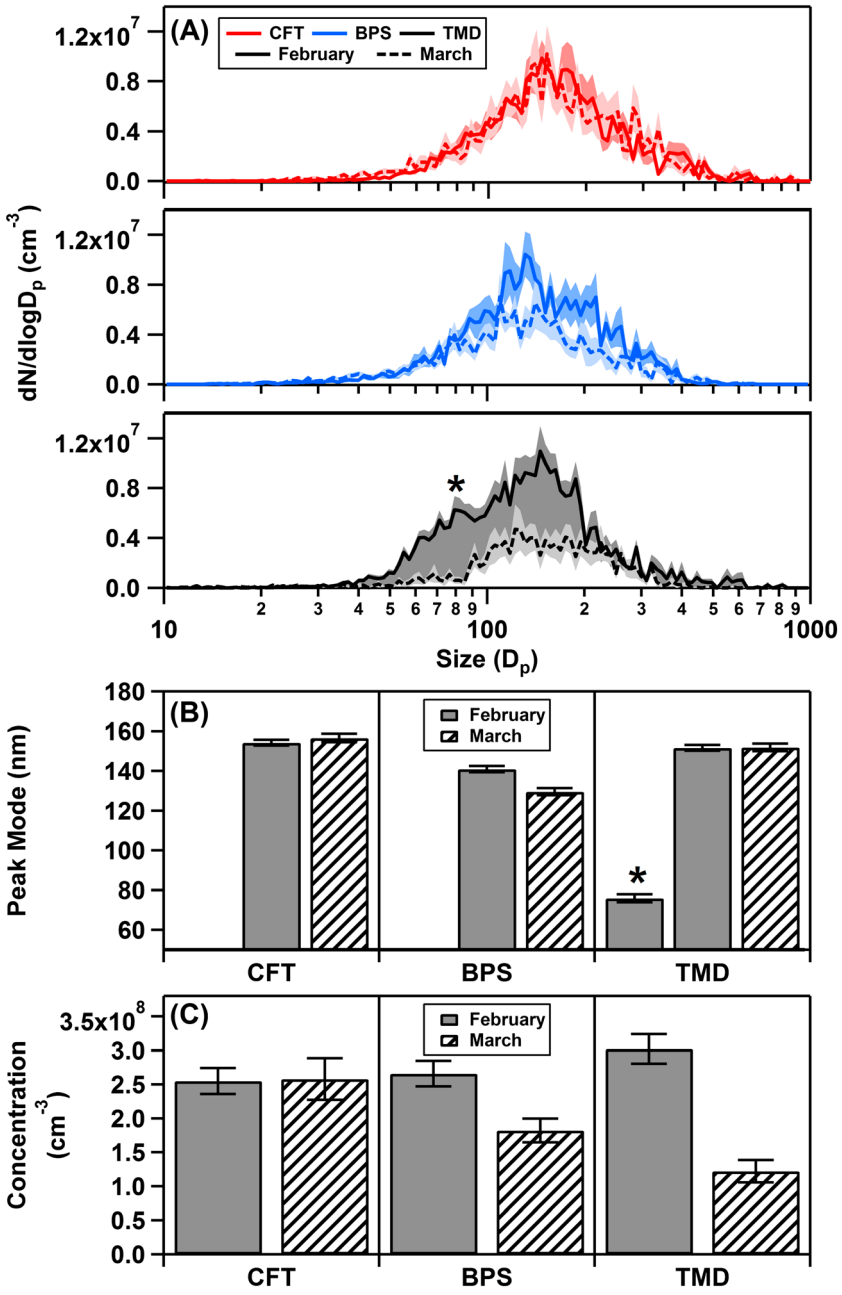

Figure 2. (a) Insoluble residue size distributions for each of the snow melt samples (February, solid line and March, dashed line). The asterisk denotes the secondary peak observed at 76 ± 2 nm. Shaded regions indicate the ± 1 standard error of the mean (February, darker sharing; March, lighter shading). The (b) mean peak mode sizes and (c) total number concentrations for each sample. Error bars show 1 standard deviation.

8000 m above ground level (m AGL). Overall, analysis included 288, 192, and 288 total back trajectories for CFT, BPS, and TMD, respectively. A limiting factor when using HYSPLIT trajectories is that they do not include processes that may affect particle concentrations, such as convective transport, wet removal, or dry removal, and are only intended to highlight the possible transport pathways. Fine particulate mass concentrations ($PM_{2.5}$; $\mu g\, m^{-3}$) measured at a site in Yosemite and sites downslope of Yosemite in the Central Valley (CV) were utilized to corroborate the potential regional sources of the aerosol components within the snow samples (see supporting information).

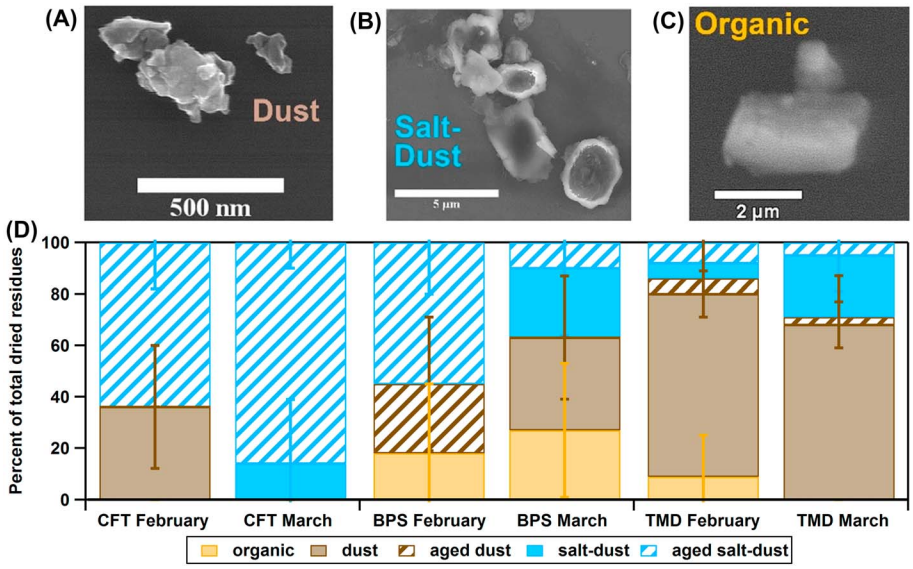

Figure 3. Representative SEM images of dried residues types including (a) dust, (b) salt-dust, and (c) organics. (d) The relative contribution from each of the dried residue types observed with EDX at each site. Solid bars represent natural aerosols, while patterned bars represent anthropogenic influenced residues. Error bars represent standard error.

3. Results

3.1. Sizing of Submicron Insoluble Residues in Melted Snow

Insoluble residue size distributions and average total number concentrations from the melted snow samples for all three sites are shown in Figure 2. At the lowest elevation site, CFT, similar peak size modes (154 ± 1 and 157 ± 2 nm, respectively), and total number concentrations ($2.6 \pm 0.2 \times 10^8$ and $2.6 \pm 0.3 \times 10^8$ cm^{-3}) were observed for the two samples collected. The higher elevation sites, BPS and TMD, however, showed more variation in peak mode and total number concentration between their two respective samples. For BPS, the size mode and average total number concentration varied between the two samples: 141 ± 2 nm and $2.7 \pm 0.2 \times 10^8$ cm^{-3}, respectively, for the first sample and 130 ± 2 nm and $1.8 \pm 0.2 \times 10^8$ cm^{-3}, respectively, for the second sample. TMD was interesting in that both the first and second samples contained the same peak mode at 152 ± 2 nm, but the first sample additionally contained a smaller mode at 76 ± 2 nm. This smaller mode could indicate influences from a different, potentially more local, source as compared to the lower elevation sites or from the March sample. The first TMD sample also had correspondingly higher number concentrations ($3.0 \pm 0.2 \times 10^8$ cm^{-3}) than the second sample ($1.2 \pm 0.2 \times 10^8$ cm^{-3}). These results indicate that the size and concentration of particles incorporated in snow at the different elevations can vary. The size distributions and total number concentrations of submicron insoluble residues provide important information that, when used in combination with chemical information, offers valuable insight regarding potential sources and atmospheric processing of aerosols impacting orographic precipitation.

3.2. Chemical Analysis of Individual Dried Residues

SEM/EDX was used to determine elemental composition of dried residues, providing source information. Representative SEM images of dried residue types identified in the melted snow included organic, dust, and salt-dust residues (Figures 3a–3c). Organic dried resides were identified as containing only C and O, which has no interference from the substrate, since Si wafers were used, whereas the dust, salt-dust, aged dust, and aged salt-dust residues were determined using a combination of elemental composition and morphology. Dust residues, which are considered here to be insoluble residues, contained several crustal elements including Al, Ti, Si, Ca, and Fe and had fractal morphology, similar to what has been previously identified as dust [*Ault et al.*, 2012; *Chen et al.*, 2012; *Krueger et al.*, 2004; *Kumar et al.*, 2012; *Lagudu et al.*, 2011; *Laskin et al.*, 2005]. Salt-dust was identified primarily by the presence of Na and Cl, mostly likely from precipitated salts formed from the drying, along with crustal elements [*Ault et al.*, 2013c], which are very distinct from anthropogenic metals [*Guasco et al.*, 2013]. Aging was determined by the presence of S, which

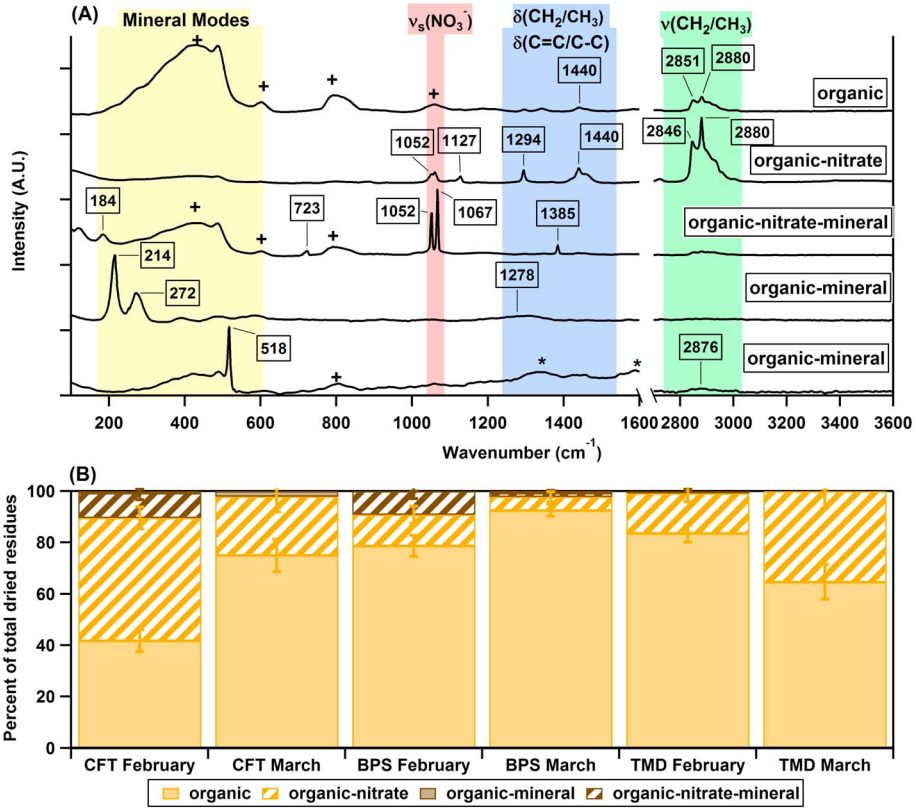

Figure 4. (a) Characteristic spectra of the dried residue types identified from the melted snow samples using the Raman microspectrometer. Major peaks used for residue classification are highlighted and labeled, with the cross indicating the quartz substrate peaks and asterisk indicating burning. (b) The relative contributions of each dried residue type for each snow melt sample created using the collected Raman spectra. Error bars represent standard error.

was presumed to be from anthropogenic pollution in the CV, namely sulfate (N from nitrate is identified by Raman below). For each of the samples, dust-containing residues comprised the majority of the dried residues observed (73–100%), with much less contribution from organic particles at each site (up to 27% at BPS). The majority of the CFT samples contained salt-dust residues (64–100%), whereas BPS and TMD contained less (36–55% and 15–29%, respectively). This indicates that clouds precipitating at CFT were influenced by marine sources. TMD showed different trends in residue types in comparison with the lower elevation sites, containing primarily dust that had not been aged (68–71%), which was most likely long-range transported from overseas. BPS samples did contain more dust residues in the samples collected in March —consistent with the spring transport of dust from Asia and Africa [*Creamean et al.*, 2013]. The varying particle compositions indicate different sources and processing of particles participating in orographic precipitation as a function of elevation.

Raman microspectroscopy provided information regarding chemical functional groups present within the dried resides of the melted snow samples. Vibrational frequencies most commonly observed for the dried residues included modes from nitrate ($\nu(NO_3^-)$), organic carbon (ν(C−H) and $\delta(CH_2/CH_3)$), and minerals (Figure 4a). Dried residues were grouped into four types which included organics, organic-nitrate, organic-mineral, and organic-nitrate-mineral (Figure 4b). The identification of sea salt and dust was particularly challenging with the Raman as there are few distinctly identifiable vibrationally active species in sea-salt aerosol (amorphous NaCl, for example, does not have a strong Raman spectrum or identifiable peaks) and fluorescence interfered with most mineral modes due to the laser wavelength (532 nm). The presence of mixtures with nitrate indicates influence from anthropogenic pollution on the residues. CFT residues had the largest amount of nitrate-containing residues, with an average of 48% for the two sampling periods (Figure S3). This site is at the lowest elevation and close to the CV, which is known to be a source of anthropogenic nitrate from urban, industrial, and agricultural emissions [*Collett et al.*, 1990; *Herckes et al.*, 2015]. BPS and TMD samples

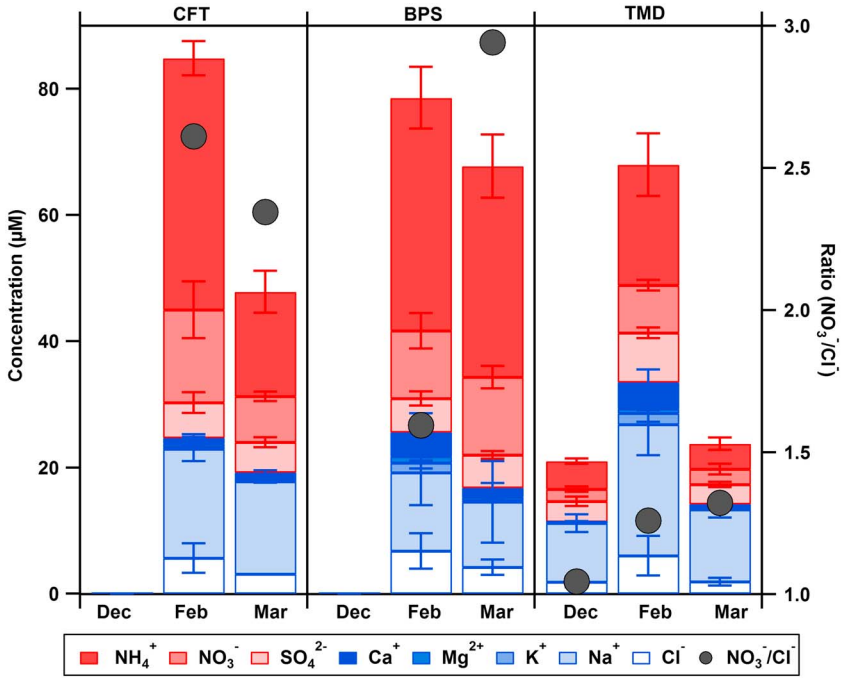

Figure 5. The concentrations of cations and anions identified using IC from each snow melt sample. Primarily, anthropogenic (red) ions and natural (blue) ions are provided in varying shades. The ratio of NO_3^- to Cl^- for each site and month is provided to indicate the chemical aging. Error bars represent standard deviation.

had lower fractions of nitrate-containing residues, at an average of 13 and 22% for both sampling periods, respectively. Though CFT showed the largest concentration of dust-containing residues, this was still only around 8% of the total particles, and the SEM/EDX dust fractions are considered more reliable. The greater sulfate- and nitrate-containing fractions for the lower elevation site (CFT) versus the higher sites emphasizes the decreasing effect of regional pollution and increasing impact of long-range transport for in-cloud aerosol composition as elevation increases.

3.3. Bulk Soluble Ion Chemistry

Bulk soluble ions from the melted snow samples were identified and quantified using IC to corroborate potential sources and aging of soluble components associated with the insoluble residues, such as nitrate or sulfate uptake on mineral dust (Figure 5). Ions identified as secondary species are SO_4^{2-}, NO_3^-, and NH_4^+, and those which are attributed to primary, natural sources include Ca^{2+}, Mg^{2+}, K^+, Cl^-, and Na^+ (i.e., known tracers for mineral dust, sea salt, and/or biomass burning). NH_4^+ and NO_3^- correlated strongly ($r^2 = 0.95$) and likely originated from pollution in the CV (Figure S4). Cleaner conditions (i.e., low concentrations of all ions) were observed at TMD relative to the lower elevation sites during most of the sample collection time periods, particularly for the March sample collection. The December sample also was collected during clean conditions, i.e., had the lowest concentrations of all ions. These results align with those from SEM/EDX and Raman, demonstrating the influence of regional CV pollutants at lower elevations. Fairly strong correlations ($0.6 \leq r^2 < 0.7$) existed for Na^+ and SO_4^{2-} ($r^2 = 0.69$), K^+ and Cl^- ($r^2 = 0.64$), and K^+ and SO_4^{2-} ($r^2 = 0.61$), with the dominant sources of these species likely being from local biomass burning. These ions additionally have fairly strong correlations with crustal species, such as Ca^{2+}, Mg^{2+}, and NH_4^+, suggesting they may also have contributions from crustal material and, less likely, from CV pollution. The correlation between Na^+ and Cl^- was weak ($r^2 = 0.35$), suggesting that (1) fresh sea salt was not a strong contributor to the snow chemistry, (2) sea salt was aged or cloud processed ($r^2 = 0.65$ between Na^+ and SO_4^{2-}), and/or (3) a portion of the Na^+ originated from other types of aerosols, such as the soluble content of mineral dust or biomass burning [*Ooki and Uematsu*, 2005; *Silva et al.*, 1999]. In addition, the ratio of Na^+ to Mg^{2+} for all samples was observed to range from 12:1 to 120:1, which is greater than the 10:1 in seawater, further corroborating that these ions did not solely originate from a marine source [*Pilson*, 1998].

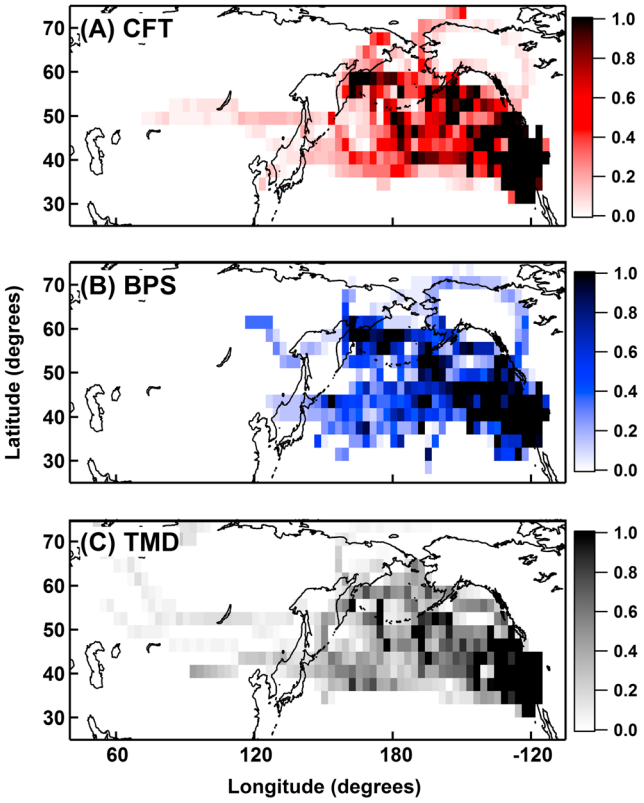

Figure 6. Air mass back trajectories calculated for (a–c) all three Yosemite snow sampling sites calculated using HYSPLIT at 1000 m AGL. The color scales represent the fraction of trajectory endpoints in each cell over the total number of HYSPLIT trajectories per atmospheric level and per sample collection time period.

Previous studies have shown that primary biomass burning, sea salt, or dust particles can undergo heterogeneous reactions in the atmosphere with gases such as $HNO_{3(g)}$ and/or $N_2O_{5(g)}$, which in the case of sea salt, can displace chloride with nitrate [*Ault et al.*, 2013b, 2014; *Gard et al.*, 1998; *Lee et al.*, 2011; *Saul et al.*, 2006]. Therefore, the amount of NO_3^- relative to Cl^- is indicative of the extent of particle aging, with more Cl^- signifying less-aged particles and more NO_3^- signifying aged aerosol [*Ault et al.*, 2014; *Gard et al.*, 1998]. While Figure 5 shows that greater aging (red shaded ions) occurred at the lower elevations sites due to their proximity to the CV, with less aging at TMD, higher nitrate levels could also signify more scavenging of $HNO_{3(g)}$, $N_2O_{5(g)}$, or nitrate-containing particles at lower elevation sites by falling snow [*Chan and Chung*, 1986; *Chang*, 1984]. Overall, the results from the soluble ion analysis corroborate the sources and extent of particle aging at each site determined by insoluble particle characterization.

3.4. Sources of Yosemite Snow Residues

Air mass back trajectories provided complementary information by showing the history and probable source regions of the air masses which contained the particles that were transported to Yosemite. Figure 6 shows the trajectory pathways for each of the three Yosemite snow sampling sites. Trajectories shown were run 10 days back in time at a starting elevation of 1000 m AGL, and darker colors indicate a higher fraction of trajectories that pass through a cell. Ten days was chosen as it has previously been demonstrated that aerosols originating from Asia, and even as far back as Africa, are transported to the western U.S. [*Ault et al.*, 2011; *Creamean et al.*, 2014a]. Further, *Uno et al.* [2009] have shown that aerosols originating from Asia can be transported in one full circuit around the Earth in 13 days at 8–10 km in altitude. The fraction of trajectories representing long-range transport from Asia or Africa (defined as $< 145°$ longitude) was ~3 times greater for TMD than CFT and 2.4 times higher for TMD than BPS, indicating that TMD had greater long-range transport. This was cross checked at 5000 m AGL for each site and similar trends observed (data not shown). The trajectories followed both meridional and zonal transport across the Pacific Ocean. These meridional and zonal pathways were similar to those observed by *Creamean et al.* [2014a] and *Uno et al.* [2008] during the spring when long-range dust transport is prevalent. This source analysis supports the observation of greater unaged dust at TMD in comparison to BPS and CFT.

4. Discussion

The combination of insoluble residue size, dried residue size and chemistry, bulk soluble ion chemistry, and air mass trajectories enabled the identification of the sources and extent of aging of aerosols involved in aerosol-cloud-precipitation interactions in the Sierra Nevada. Evaluating the size and chemical composition of insoluble residues found in snow provides information on the potential INPs involved with cloud glaciation and may also indicate the types of aerosols scavenged by descending snow crystals. These results demonstrate that the sources and atmospheric processing of insoluble residues vary significantly as a function of

elevation, even over relatively small spatial scales. Of particular note was a transition from anthropogenic to natural influences observed as a function of increasing elevation.

The lowest elevation site, CFT (1900 m AMSL), was characterized by consistent submicron residue size and number concentration between the samples, as compared to the variability between the BPS (2200 m AMSL) and TMD (2600 m AMSL) samples, indicating similar sources at CFT during sample collection (Figure 2). Although CFT and BPS are hypothesized to be heavily influenced by the CV, the difference in size between BPS and CFT may be attributed to the samples from CFT undergoing a greater extent of aging or more scavenging of pollutant species by falling snow crystals, creating coatings that lead to larger sizes, either from the seed aerosols or formed during the drying process. BPS is higher in elevation, and thus may be exposed to a variety of sources, as reflected by the sizing and compositional analyses. For example, the ratio of NO_3^- to Cl^- is fairly consistent between the CFT samples (and high) but highly variable between the BPS samples (Figure 5). It is important to note that each of the techniques utilized in this work measure different size ranges (Table 1) and therefore will not always render similar trends. However, these techniques can be used in combination to develop a picture of the entire aerosol population and the sources/extent of aging within different size ranges. Further, although BPS is higher in elevation than CFT, it is closer by distance to the CV and thus appeared at times to be exposed to as much or more anthropogenic influence (BPS and CFT are ~50 and ~64 km from the CV floor, respectively, while only varying in elevation by 300 m). CV pollutants were also particularly low at TMD, when compared to the other sites, suggesting that it was less exposed to CV pollutants, as demonstrated by the NO_3^-/Cl^- ratio (Figure 5). Less influence from pollution on the insoluble residues in the snow was observed at TMD, particularly for the March sample, which was expected based on its distance from the CV (TMD is ~80 km from the CV floor and 400–700 m higher than the other two sites).

CV pollution was transported upslope to Yosemite and either (1) incorporated into the cloud base or (2) scavenged by falling snow during collection. Rosenfeld and colleagues have shown that high concentrations of pollution aerosols that serve as cloud condensation nuclei (CCN) from urban areas in the CV suppress precipitation on the windward side of the Sierra Nevada [*Givati and Rosenfeld*, 2004; *Rosenfeld and Givati*, 2006]. Additionally, particles which acquire secondary species from pollution sources have been shown to increase in hygroscopicity as compared to the original, more hydrophobic core, increasing CCN capabilities [*Petters et al*., 2006; *Wang et al*., 2010]. Combined, these previous studies demonstrate the importance of understanding to what extent aerosols are aged and when they are incorporated into orographic clouds above the Sierra barrier. In the current study, Raman showed a strong influence from organic/nitrate-containing particles (Figure 4b), likely from aging in the CV and during transport to the site. Further, the strong correlation between ammonium and nitrate concentrations (from IC) in the Yosemite samples supports the coorigin of these species from agricultural sources of the CV [*Zhang and Anastasio*, 2001] (Figure 5). Nitrate could also be from aged mineral dust or other aerosols during transport at higher altitudes.

TMD was more chemically distinct from the lower elevation sites due to its higher elevation and greater exposure to long-range transport conditions. Number concentrations of insoluble residues in solution varied between samples more at higher elevation sites, particularly at TMD, suggesting less consistent sources than the lowest elevation sites. During the time period where the samples were collected, a transition to more efficient long-range transport, particularly of dust from overseas, occurs in this region. Long-range transported mineral dust has been deemed a frequent and important contributor to Sierra Nevada precipitation [*Ault et al*., 2011; *Creamean et al*., 2014a, 2015, 2013; *Fan et al*., 2014], particularly starting in March. The change to greater concentration of dust residues and less influence from local pollution sources was reflected in the number concentrations of submicron particles, in addition to the residue chemistry. Submicron number concentrations were lower, and the smaller-size mode was not present at TMD during the March sampling, likely due to less influence from smaller particles from pollution sources and more influence from larger dust particles. SEM/EDX results corroborate this, showing a change to dust at TMD (Figure 3d). IC (Figure S4) also showed strong correlations among ions commonly associated with crustal material, Ca^{2+}, Mg^{2+}, and K^+ [*Sorooshian et al*., 2013; *Wang et al*., 2005]. While dust was prominent in the SEM/EDX residue analysis, concentrations of dissolved Ca^{2+} and Mg^{2+} were not always highest at TMD. The low concentrations of soluble Ca^{2+} and Mg^{2+} was likely a result of less aged or heterogeneously processed dust, particularly during the March sample collection, which would prevent dissolution of insoluble mineral species [*Savoie and Prospero*, 1980; *Wang et al*., 2005]. Cloud processing of the mineral dust can have implications for modulating INP properties of the dust, subsequently impacting its role in ice and

precipitation formation processes in Sierra Nevada orographic clouds [*Cziczo et al*., 2009; *Sullivan et al*., 2007, 2010]. Additionally, Ca^{2+} and Mg^{2+} were strongly correlated with Cl^- and SO_4^{2-}, indicating that the dust may have been cloud processed with marine air (and inorganic ions from sea salt) during transport or underwent riming during precipitation.

The smaller-size mode present in the February TMD sample (Figure 2) in conjunction with the presence of pollutant ions (Figure 5) indicates a potentially unique, more local pollution source at TMD during this time period as compared to the lower elevation sites or the remaining TMD samples. Typically, TMD samples contained less pollutant ions (i.e., NH_4^+, NO_3^-, and SO_4^{2-}), apart from the February sample, indicating the air at TMD was cleaner than the sites closest to the CV. Clouds influenced by clean marine air masses have been shown to contribute to precipitation formation in the Sierra Nevada due to warm rain processes during atmospheric rivers or through the seeder-feeder mechanism, whereby ice formed in the overlaying "feeder" cloud falls into the "seeder" cloud [*Creamean et al*., 2013; *Meyers et al*., 1992; *White et al*., 2015]. The seeder cloud, if influenced by marine sources, can contain large liquid droplets that collect on the surface of the descending ice crystals, enabling them to grow rapidly into snowflakes and descend toward the ground. Thus, sea-salt aerosols can create pristine clouds that, under certain conditions, can serve to enhance precipitation formation [*Posselt and Lohmann*, 2008; *Yin et al*., 2000].

Overall, these results indicate that CFT and BPS were commonly exposed to CV pollutants, while less pollutant species were observed at the higher and more isolated TMD. TMD was variable in that the snow was impacted by both long-range transported and, to a smaller extent, local pollution sources during the February sampling time period and then predominantly long-range transport during the March sampling time period. These elevation trends suggest removal of pollutants at the lower elevations occurs because they are closer to the CV, and orographic storm systems hit these locations first. *Collett et al*. [1990] observed a similar trend, with concentrations of major pollution ion species (i.e., NH_4^+, NO_3^-, and SO_4^{2-}) in cloud water decreasing with elevation in the central Sierra Nevada. Our results demonstrate how variable precipitation chemistry; and thus, aerosol-cloud-precipitation effects can vary on such a small spatial scale. *Creamean et al*. [2015] reported that precipitation residues collected at sites throughout the Sierra Nevada were strongly correlated to cloud ice and precipitation phase and quantity, demonstrating the importance of evaluating precipitation residues in mountain regions.

5. Conclusions

Improving our understanding of the detailed physiochemical properties and sources of aerosols that influence snowfall in Yosemite has important implications for snowpack in the Sierra Nevada in terms of how these aerosols serve as INPs. The chemical composition and size of particle-phase components found in snow samples collected at three locations of variable elevation provided insight into the sources of aerosols that potentially influence precipitation formation over Yosemite National Park. The size and chemical composition of individual residues, which determined the sources and extent of aging of insoluble residues, were observed to vary depending on where (and when) the samples were collected and were corroborated by bulk soluble ion analysis. TMD samples were predominantly influenced by clean, marine air off the coast of California and subject to long-range transport of mineral dust, particularly during the second event. In contrast, lower elevation sites, CFT and BPS, showed greater influence from CV pollution as indicated by the presence of ammonium and nitrate ions. The transition in aerosol sources that impact clouds above the Sierra Nevada has implications for controlling, to an extent, the phase and quantity of precipitation [*Creamean et al*., 2016]. Subsequent snowfall influenced by aerosols that form cloud ice increases the snowpack in the Sierra Nevada region and supplies a steady source of water for California throughout the spring. Thus, understanding all the components that affect this snowpack is vital for water resources management. In the future, results such as these could be used for regional weather and climate models to assess aerosol impacts on snowpack in the Sierra Nevada and mountainous regions beyond [*Bauer et al*., 2013].

Acknowledgments

The authors would like to acknowledge the Yosemite National Park Service staff who helped with snow sample collection, particularly Katy Warner, who organized collection at Yosemite, Rebecca Rising, and Rob and Laura Pilewski. The authors would like to acknowledge Martin Philbert of the School of Public Health at the University of Michigan, Andrew Maynard, and Sonja Capracotta at Malvern Instrument in Westborough, Massachusetts for use of the NanoSight™ LM10 instrument. The Michigan Center for Materials Characterization $(MC)^2$ at the University of Michigan is acknowledged for assistance with electron microscopy. The authors acknowledge the NOAA Air Resources Laboratory (ARL) for the provision of the HYSPLIT transport and dispersion model and READY website (www.arl.noaa.gov/ready.php) used in this paper. We also thank CARB for availability of particulate mass concentration measurements in the CV and Yosemite. J. Creamean was partially funded by the National Research Council Research Associate Program. Support for M. Weber was provided by the National Science Foundation (NSF) Research Experience for Undergraduates (REU) (CHE-1062654) at the University of Michigan-Department of Chemistry. Data presented in this paper can be obtained upon request by contacting one of the corresponding authors, J. Creamean (jessie.creamean@noaa.gov) or A. Ault (aulta@umich.edu).

References

Andreae, M. O., and D. Rosenfeld (2008), Aerosol-cloud-precipitation interactions. Part 1. The nature and sources of cloud-active aerosols, *Earth Sci. Rev.*, *89*(1-2), 13–41.

Ault, A. P., C. R. Williams, A. B. White, P. J. Neiman, J. M. Creamean, C. J. Gaston, F. M. Ralph, and K. A. Prather (2011), Detection of Asian dust in California orographic precipitation, *J. Geophys. Res.*, *116*, D16205, doi:10.1029/2010JD015351.

Ault, A. P., T. M. Peters, E. J. Sawvel, G. S. Casuccio, R. D. Willis, G. A. Norris, and V. H. Grassian (2012), Single-particle SEM-EDX analysis of iron-containing coarse particulate matter in an urban environment: Sources and distribution of iron within Cleveland, Ohio, *Environ. Sci. Technol.*, *46*(8), 4331–4339.

Ault, A. P., D. Zhao, C. J. Ebben, M. J. Tauber, F. M. Geiger, K. A. Prather, and V. H. Grassian (2013a), Raman microspectroscopy and vibrational sum frequency generation spectroscopy as probes of the bulk and surface compositions of size-resolved sea spray aerosol particles, *Phys. Chem. Chem. Phys.*, *15*(17), 6206–6214.

Ault, A. P., T. L. Guasco, O. S. Ryder, J. Baltrusaitis, L. A. Cuadra-Rodriguez, D. B. Collins, M. J. Ruppel, T. H. Bertram, K. A. Prather, and V. H. Grassian (2013b), Inside versus Outside: Ion redistribution in nitric acid reacted sea spray aerosol particles as determined by single particle analysis, *J. Am. Chem. Soc.*, *135*(39), 14,528–14,531.

Ault, A. P., et al. (2013c), Size-dependent changes in sea spray aerosol composition and properties with different seawater conditions, *Environ. Sci. Technol.*, *47*(11), 5603–5612.

Ault, A. P., T. L. Guasco, J. Baltrusaitis, O. S. Ryder, J. V. Trueblood, D. B. Collins, M. J. Ruppel, L. A. Cuadra-Rodriguez, K. A. Prather, and V. H. Grassian (2014), Heterogeneous reactivity of nitric acid with nascent sea spray aerosol: Large differences observed between and within individual particles, *J. Phys. Chem. Lett.*, *5*(15), 2493–2500.

Axson, J. L., J. M. Creamean, A. L. Bondy, S. S. Capracotta, K. Y. Warner, and A. P. Ault (2014), An in situ method for sizing insoluble residues in precipitation and other aqueous samples, *Aerosol Sci. Technol.*, *49*(1), 24–34.

Axson, J. L., H. Shen, A. L. Bondy, C. C. Landry, J. Welz, J. M. Creamean, and A. P. Ault (2016), Transported mineral dust deposition case study at a hydrologically sensitive mountain site: Size and composition shifts in ambient aerosol and snowpack, *Aerosol Air Qual. Res.*, *16*(3), 555–567.

Bauer, S. E., A. Ault, and K. A. Prather (2013), Evaluation of aerosol mixing state classes in the GISS modelE-MATRIX climate model using single-particle mass spectrometry measurements, *J. Geophys. Res. Atmos.*, *118*, 9834–9844, doi:10.1002/jgrd.50700.

Bergeron, T. (1935), On the physics of cloud and precipitation, in *Proceedings of the 5th Assembly of the U.G.G.I*, pp. 156–178, Paul Dupont, Paris.

Borys, R. D., D. H. Lowenthal, and D. L. Mitchell (2000), The relationships among cloud microphysics, chemistry, and precipitation rate in cold mountain clouds, *Atmos. Environ.*, *34*(16), 2593–2602.

Chan, W. H., and D. H. S. Chung (1986), Regional-scale precipitation scavenging of SO_2, SO_4, NO_3 and HNO_3, *Atmos. Environ.*, *20*(7), 1397–1402.

Chang, T. Y. (1984), Rain and snow scavenging of HNO_3 vapor in the atmosphere, *Atmos. Environ.*, *18*(1), 191–197.

Chen, H., A. Laskin, J. Baltrusaitis, C. A. Gorski, M. M. Scherer, and V. H. Grassian (2012), Coal fly ash as a source of iron in atmospheric dust, *Environ. Sci. Technol.*, *46*(4), 2112–2120.

Christner, B. C., R. Cai, C. E. Morris, K. S. McCarter, C. M. Foreman, M. L. Skidmore, S. N. Montross, and D. C. Sands (2008), Geographic, seasonal, and precipitation chemistry influence on the abundance and activity of biological ice nucleators in rain and snow, *Proc. Natl. Acad. Sci. U. S. A.*, *105*(48), 18,854–18,859.

Collett, J. L., B. C. Daube, D. Gunz, and M. R. Hoffmann (1990), Intensive studies of Sierra Nevada cloudwater chemistry and its relationship to precursor aerosol and gas concentrations, *Atmos. Environ., Part A*, *24*(7), 1741–1757.

Craig, R. L., A. L. Bondy, and A. P. Ault (2015), Surface enhanced Raman spectroscopy enables observations of previously undetectable secondary organic aerosol components at the individual particle level, *Anal. Chem.*, *87*(15), 7510–7514.

Creamean, J. M., et al. (2013), Dust and biological aerosols from the Sahara and Asia influence precipitation in the western U.S, *Science*, *339*(6127), 1572–1578.

Creamean, J. M., J. R. Spackman, S. M. Davis, and A. B. White (2014a), Climatology of long-range transported Asian dust along the West Coast of the United States, *J. Geophys. Res. Atmos.*, *119*, 12,171–12,185, doi:10.1002/2014JD021694.

Creamean, J. M., C. Lee, T. C. Hill, A. P. Ault, P. J. DeMott, A. B. White, F. M. Ralph, and K. A. Prather (2014b), Chemical properties of insoluble precipitation residue particles, *J. Aerosol Sci.*, *76*, 13–27.

Creamean, J. M., A. P. Ault, A. B. White, P. J. Neiman, F. M. Ralph, P. Minnis, and K. A. Prather (2015), Impact of interannual variations in sources of insoluble aerosol species on orographic precipitation over California's central Sierra Nevada, *Atmos. Chem. Phys.*, *15*(11), 6535–6548.

Creamean, J. M., A. B. White, P. Minnis, R. Palikonda, D. A. Spangenberg, and K. A. Prather (2016), The relationships between insoluble precipitation residues, clouds, and precipitation over California's southern Sierra Nevada during winter storms, *Atmos. Environ.*, *140*, 298–310.

Croft, B., U. Lohmann, R. V. Martin, P. Stier, S. Wurzler, J. Feichter, R. Posselt, and S. Ferrachat (2009), Aerosol size-dependent below-cloud scavenging by rain and snow in the ECHAM5-HAM, *Atmos. Chem. Phys.*, *9*(14), 4653–4675.

Croft, B., U. Lohmann, R. V. Martin, P. Stier, S. Wurzler, J. Feichter, C. Hoose, U. Heikkila, A. van Donkelaar, and S. Ferrachat (2010), Influences of in-cloud aerosol scavenging parameterizations on aerosol concentrations and wet deposition in ECHAM5-HAM, *Atmos. Chem. Phys.*, *10*(4), 1511–1543.

Cziczo, D. J., K. D. Froyd, S. J. Gallavardin, O. Moehler, S. Benz, H. Saathoff, and D. M. Murphy (2009), Deactivation of ice nuclei due to atmospherically relevant surface coatings, *Environ. Res. Lett.*, *4*(4, 044013), doi:10.1088/1748-9326/4/4/044013.

Dettinger, M. D., F. M. Ralph, T. Das, P. J. Neiman, and D. R. Cayan (2011), Atmospheric rivers, floods and the water resources of California, *Water*, *3*(2), 445–478.

Draxler, R. R., and G. D. Rolph (2011), HYSPLIT (HYbrid Single-Particle Lagrangian Integrated Trajectory) model access via NOAA ARL READY website. [Available at http://ready.arl.noaa.gov/HYSPLIT.phpedited, NOAA Air Resources Laboratory, Silver Spring, Md.]

Fan, J., et al. (2014), Aerosol impacts on California winter clouds and precipitation during CalWater 2011: Local pollution versus long-range transported dust, *Atmos. Chem. Phys.*, *14*(1), 81–101.

Gard, E. E., et al. (1998), Direct observation of heterogeneous chemistry in the atmosphere, *Science*, *279*(5354), 1184–1187.

Givati, A., and D. Rosenfeld (2004), Quantifying precipitation suppression due to air pollution, *J. Appl. Meteorol.*, *43*(7), 1038–1056.

Givati, A., and D. Rosenfeld (2007), Possible impacts of anthropogenic aerosols on water resources of the Jordan River and the Sea of Galilee, *Water Resour. Res.*, *43*, W10419, doi:10.1029/2006WR005771.

Guan, B., D. E. Waliser, N. P. Molotch, E. J. Fetzer, and P. J. Neiman (2012), Does the Madden-Julian Oscillation influence wintertime atmospheric rivers and snowpack in the Sierra Nevada? *Mon. Weather Rev.*, *140*(2), 325–342.

Guasco, T. L., et al. (2013), Transition metal associations with primary biological particles in sea spray aerosol generated in a wave channel, *Environ. Sci. Technol.*, *48*(11), 1324–1333.

Hallett, J., R. I. Sax, D. Lamb, and A. S. R. Murty (1978), Aircraft measurements of ice in Florida cumuli, *Q. J. R. Meteorol. Soc.*, *104*(441), 631–651.

Henning, S., E. Weingartner, M. Schwikowski, H. W. Gaggeler, R. Gehrig, K. P. Hinz, A. Trimborn, B. Spengler, and U. Baltensperger (2003), Seasonal variation of water-soluble ions of the aerosol at the high-alpine site Jungfraujoch (3580 m asl), *J. Geophys. Res.*, *108*(D1), 4030, doi:10.1029/2002JD002439.

Herckes, P., A. R. Marcotte, Y. Wang, and J. L. Collett (2015), Fog composition in the Central Valley of California over three decades, *Atmos. Res.*, *151*, 20–30.
Holecek, J. C., M. T. Spencer, and K. A. Prather (2007), Analysis of rainwater samples: Comparison of single particle residues with ambient particle chemistry from the northeast Pacific and Indian oceans, *J. Geophys. Res.*, *112*, D22S24, doi:10.1029/2006JD008269.
Kalnay, E., et al. (1996), The NCEP/NCAR 40-year reanalysis project, *Bull. Am. Meteorol. Soc.*, *77*(3), 437–471.
Kasper-Giebl, A., M. F. Kalina, and H. Puxbaum (1999), Scavenging ratios for sulfate, ammonium and nitrate determined at Mt. Sonnblick (3106 m asl), *Atmos. Environ.*, *33*(6), 895–906.
Klein, H., et al. (2010), Saharan dust and ice nuclei over Central Europe, *Atmos. Chem. Phys.*, *10*(21), 10,211–10,221.
Krueger, B. J., V. H. Grassian, J. P. Cowin, and A. Laskin (2004), Heterogeneous chemistry of individual mineral dust particles from different dust source regions: The importance of particle mineralogy, *Atmos. Environ.*, *38*(36), 6253–6261.
Kumar, P., P. K. Hopke, S. Raja, G. Casuccio, T. L. Lersch, and R. R. West (2012), Characterization and heterogeneity of coarse particles across an urban area, *Atmos. Environ.*, *46*, 449–459.
Lafreniere, M. J., and K. E. Sinclair (2011), Snowpack and precipitation chemistry at a high altitude site in the Canadian Rocky Mountains, *J. Hydrol.*, *409*(3-4), 737–748.
Lagudu, U. R. K., S. Raja, P. K. Hopke, D. C. Chalupa, M. J. Utell, G. Casuccio, T. L. Lersch, and R. R. West (2011), Heterogeneity of coarse particles in an urban area, *Environ. Sci. Technol.*, *45*(8), 3288–3296.
Laskin, A., T. W. Wietsma, B. J. Krueger, and V. H. Grassian (2005), Heterogeneous chemistry of individual mineral dust particles with nitric acid: A combined CCSEM/EDX, ESEM, and ICP-MS study, *J. Geophys. Res.*, *110*, D10208, doi:10.1029/2004JD005206.
Lee, M.-J., H.-J. Jung, H.-J. Eom, S. Maskey, H. K. Kim, and C.-U. Ro (2011), Hygroscopic behavior of individual $NaNO_3$ particles, *Atmos. Chem. Phys. Discuss.*, *11*, 23,203–23,229.
Lynn, B., A. Khain, D. Rosenfeld, and W. L. Woodley (2007), Effects of aerosols on precipitation from orographic clouds, *J. Geophys. Res.*, *112*, D10225, doi:10.1029/2006JD007537.
Ma, C. J., S. Tohno, M. Kasahara, and S. Hayakawa (2004), Properties of the size-resolved and individual cloud droplets collected in western Japan during the Asian dust storm event, *Atmos. Environ.*, *38*(27), 4519–4529.
Matthias-Maser, S., B. Bogs, and R. Jaenicke (2000), The size distribution of primary biological aerosol particles in cloud water on the mountain Kleiner Feldberg/Taunus(FRG), *Atmos. Res.*, *54*(1), 1–13.
Meyers, M. P., P. J. Demott, and W. R. Cotton (1992), New primary ice-nucleation parameterizations in an explicit cloud model, *J. Appl. Meteorol.*, *31*(7), 708–721.
Mossop, S. C. (1970), Concentrations of ice crystals in clouds, *Bull. Am. Meteorol. Soc.*, *51*(6), 474–479.
Mossop, S. C., A. Ono, and E. R. Wishart (1970), Ice particles in maritime clouds near Tasmania, *Q. J. R. Meteorol. Soc.*, *96*(409), 487–508.
Ooki, A., and M. Uematsu (2005), Chemical interactions between mineral dust particles and acid gases during Asian dust events, *J. Geophys. Res.*, *110*(D3, D03201), doi:10.1029/2004JD004737.
Petters, M. D., A. J. Prenni, S. M. Kreidenweis, P. J. DeMott, A. Matsunaga, Y. B. Lim, and P. J. Ziemann (2006), Chemical aging and the hydrophobic-to-hydrophilic conversion of carbonaceous aerosol, *Geophys. Res. Lett.*, *33*, L24806, doi:10.1029/2006GL027249.
Pilson, M. E. Q. (1998), *An Introduction to the Chemistry of the Sea*, Prentice Hall, Upper Saddle River, N. J.
Pomeroy, J. W., T. D. Davies, and M. Tranter (1991), The impact of blowing snow on snow chemistry, in *Seasonal Snowpacks* edited by, T. D. Davies et al. pp. 71–113, Springer, Verlag.
Posselt, R., and U. Lohmann (2008), Influence of giant CCN on warm rain processes in the ECHAM5 GCM, *Atmos. Chem. Phys.*, *8*(14), 3769–3788.
Pruppacher, H. R., and J. D. Klett (1978), *Microphysics of clouds and precipitation*, Reidel, Dordecht, Neth.
Radke, L. F., P. V. Hobbs, and M. W. Eltgroth (1980), Scavenging of aerosol particles by precipitation, *J. Appl. Meteorol.*, *19*(6), 715–722.
Rodhe, H., and J. A. N. Grandell (1972), On the removal time of aerosol particles from the atmosphere by precipitation scavenging, *Tellus*, *24*(5), 442–454.
Rosenfeld, D., and A. Givati (2006), Evidence of orographic precipitation suppression by air pollution-induced aerosols in the western United States, *J. Appl. Meteorol. Climatol.*, *45*(7), 893–911.
Rosenfeld, D., W. L. Woodley, D. Axisa, E. Freud, J. G. Hudson, and A. Givati (2008), Aircraft measurements of the impacts of pollution aerosols on clouds and precipitation over the Sierra Nevada, *J. Geophys. Res.*, *113*, D15203, doi:10.1029/2007JD009544.
Rosenfeld, D., R. Chemke, K. Prather, K. Suski, J. M. Comstock, B. Schmid, J. Tomlinson, and H. Jonsson (2014), Polluting of winter convective clouds upon transition from ocean inland over central California: Contrasting case studies, *Atmos. Res.*, *135*, 112–127.
Saleeby, S. M., W. R. Cotton, D. Lowenthal, R. D. Borys, and M. A. Wetzel (2009), Influence of cloud condensation nuclei on orographic snowfall, *J. Appl. Meteorol. Climatol.*, *48*(5), 903–922.
Saul, T. D., M. P. Tolocka, and M. V. Johnston (2006), Reactive uptake of nitric acid onto sodium chloride aerosols across a wide range of relative humidities, *J. Phys. Chem. A*, *110*(24), 7614–7620.
Savoie, D. L., and J. M. Prospero (1980), Water-soluble potassium, calcium, and magnesium in the aerosols over the tropical North-Atlantic, *J. Geophys. Res.*, *85*(C1), 385–392, doi:10.1029/JC085iC01p00385.
Schumann, T., B. Zinder, and A. Waldvogel (1988), Aerosol and hydrometeor concentrations and their chemical-composition during winter precipitation along a mountain slope 1. Temporal evolution of the aerosol, microphysical and meteorological conditions, *Atmos. Environ.*, *22*(7), 1443–1459.
Schutz, L., and M. Kramer (1987), Rainwater composition over a rural area with special emphasis on the size distribution of insoluble particulate matter, *J. Atmos. Chem.*, *5*(2), 173–184.
Shen, H., T. M. Peters, G. S. Casuccio, T. L. Lersch, R. R. West, A. Kumar, N. Kumar, and A. P. Ault (2016), Elevated concentrations of lead in particulate matter on the neighborhood-scale in Delhi, India as determined by single particle analysis, *Environ. Sci. Technol.*, *50*(10), 4961–4970, doi:10.1021/acs.est.5b06202.
Shrestha, A. B., C. P. Wake, and J. E. Dibb (1997), Chemical composition of aerosol and snow in the high Himalaya during the summer monsoon season, *Atmos. Environ.*, *31*(17), 2815–2826.
Silva, P. J., D. Y. Liu, C. A. Noble, and K. A. Prather (1999), Size and chemical characterization of individual particles resulting from biomass burning of local Southern California species, *Environ. Sci. Technol.*, *33*(18), 3068–3076.
Sorooshian, A., T. Shingler, A. Harpold, C. W. Feagles, T. Meixner, and P. D. Brooks (2013), Aerosol and precipitation chemistry in the southwestern United States: Spatiotemporal trends and interrelationships, *Atmos. Chem. Phys.*, *13*(15), 7361–7379.
Sullivan, R. C., S. A. Guazzotti, D. A. Sodeman, and K. A. Prather (2007), Direct observations of the atmospheric processing of Asian mineral dust, *Atmos. Chem. Phys.*, *7*, 1213–1236.
Sullivan, R. C., et al. (2010), Irreversible loss of ice nucleation active sites in mineral dust particles caused by sulphuric acid condensation, *Atmos. Chem. Phys.*, *10*(23), 11,471–11,487.

Uno, I., K. Yumimoto, A. Shimizu, Y. Hara, N. Sugimoto, Z. Wang, Z. Liu, and D. M. Winker (2008), 3D structure of Asian dust transport revealed by CALIPSO lidar and a 4DVAR dust model, *Geophys. Res. Lett.*, *35*, L06803, doi:10.1029/2007GL032329.

Uno, I., K. Eguchi, K. Yumimoto, T. Takemura, A. Shimizu, M. Uematsu, Z. Y. Liu, Z. F. Wang, Y. Hara, and N. Sugimoto (2009), Asian dust transported one full circuit around the globe, *Nat. Geosci.*, *2*(8), 557–560.

Vali, G., P. J. DeMott, O. Mohler, and T. F. Whale (2015), Technical note: A proposal for ice nucleation terminology, *Atmos. Chem. Phys.*, *15*(18), 10,263–10,270.

Wang, J., M. J. Cubison, A. C. Aiken, J. L. Jimenez, and D. R. Collins (2010), The importance of aerosol mixing state and size-resolved composition on CCN concentration and the variation of the importance with atmospheric aging of aerosols, *Atmos. Chem. Phys.*, *10*(15), 7267–7283.

Wang, Y., G. S. Zhuang, Y. Sun, and Z. S. An (2005), Water-soluble part of the aerosol in the dust storm season—Evidence of the mixing between mineral and pollution aerosols, *Atmos. Environ.*, *39*(37), 7020–7029.

White, A. B., P. J. Neiman, J. M. Creamean, T. Coleman, F. M. Ralph, and K. A. Prather (2015), The impacts of California's San Francisco Bay area gap on precipitation observed in the Sierra Nevada during HMT and CalWater, *J. Hydrometeorol.*, *16*(3), 1048–1069.

Xiao, H., Y. Yin, L. J. Jin, Q. Chen, and J. H. Chen (2014), Simulation of aerosol effects on orographic clouds and precipitation using WRF model with a detailed bin microphysics scheme, *Atmos. Sci. Lett.*, *15*(2), 134–139.

Xu, J. Z., Z. B. Wang, G. M. Yu, X. Qin, J. W. Ren, and D. Qin (2014), Characteristics of water soluble ionic species in fine particles from a high altitude site on the northern boundary of Tibetan Plateau: Mixture of mineral dust and anthropogenic aerosol, *Atmos. Res.*, *143*, 43–56.

Yin, Y., Z. Levin, T. G. Reisin, and S. Tzivion (2000), The effects of giant cloud condensation nuclei on the development of precipitation in convective clouds—A numerical study, *Atmos. Res.*, *53*(1-3), 91–116.

Zhang, C. L., G. J. Wu, S. P. Gao, Z. P. Zhao, X. L. Zhang, L. D. Tian, Y. J. Mu, and D. Joswiak (2013), Distribution of major elements between the dissolved and insoluble fractions in surface snow at Urumqi Glacier No. 1, Eastern Tien Shan, *Atmos. Res.*, *132*, 299–308.

Zhang, Q., and C. Anastasio (2001), Chemistry of fog waters in California's Central Valley—Part 3: Concentrations and speciation of organic and inorganic nitrogen, *Atmos. Environ.*, *35*(32), 5629–5643.